Transactions of the Indian National Academy of Engineering (2022) 7:699–706
https://doi.org/10.1007/s41403-022-00319-1

ORIGINAL ARTICLE

# Unraveling the Complexities of Deformation/Damage Incurred in P91 Steel Weld Joint During Creep–Fatigue Interaction Loading at 873 K

**P. Vaishali**[1] **· Vani Shankar**[1]

Received: 15 September 2021 / Accepted: 6 January 2022 / Published online: 1 March 2022


**Abstract**

P91 steel weld joints made by multipass welding greatly alters the initial microstructure of the base metal and a thermally graded microstructure builds up across the weld joint due to its thermal sensitive nature. More so, when the weld joint is subjected to simultaneous cyclic loading and creep deformation, the initial microstructure of not only the base metal but also each constituting microstructural zone of the weld joint varies in a very complex manner depending upon the cyclic waveform employed. Four test conditions that represent four types of cyclic loading waveforms have been chosen for the present study. These are samples that were subjected to pure fatigue (without application of dwell), and samples that were exposed to an additional dwell period applied in each cycle at peak tension or peak compression or both peak tension and compression (represented as CC, 30 TH, 30 CH and 5 TCH respectively). All experiments were performed at 873 K and at $3 \times 10^{-3}$ $s^{-1}$ strain rate using total strain amplitude of $\pm 0.6\%$. Failure location shifted with the applied waveform. Microhardness line profiles on the longitudinal section of the fatigue failed samples were obtained at an inter-distance of 0.2 mm. The first-hand information obtained using this technique indicated that hardening/softening of the constituting regions of weld joint occurred to different extents and that was also waveform dependent. The microhardness correlated well with dislocation density obtained through EBSD.

**Keywords** P91 steel · Fatigue and creep–fatigue interaction · Microstructure · Microhardness · Dislocation density

## Introduction

Modified 9Cr-1Mo is steam generator material used for prototype fast breeder reactor (PFBR) and other advanced power systems. Fabrication of such large structures involves thousands of welds and as welds is weak links in any structure (Hollner et al. 2010; Shankar et al. 2014; Thomas Paul et al. 2008) and hence they require thorough stability and reliability analysis. P91 ferritic-martensitic steels are apt for steam generator application as they possess lower coefficient of thermal expansion (Klueh 2005) and better thermal conductivity as compared to the austenitic steels. However, in spite of their good mechanical properties, weld related issues (Thomas Paul et al. 2006) leading to premature failure occurs. During welding, besides the weld metal, three different zones form adjacent to the fusion zone, classification of which is based upon the different temperatures experienced, the prior austenite grain size and the difference in cooling rates (Wang and Li 2016). The three different zones are classified as coarse grain heat affected zone (CGHAZ), fine grain heat affected zone (FGHAZ) and intercritical heat affected zone (ICHAZ), each possessing different mechanical properties with respect to the unaffected base metal. When such large, welded structures experience thermal gradients due to start-ups and shutdowns, low cycle fatigue and creep–fatigue interaction condition prevails (Shankar et al. 2011; Farragher et al. 2014). It has been found earlier that failure location shifts with the applied strain amplitude-temperature-waveform combination (Shankar 2007, thesis). The present work aims to understand the reason for the shift in failure location in P91 weld joint subjected to different cyclic waveforms.

✉ P. Vaishali
vaishalithriya@gmail.com

[1] Homi Bhabha National Institute, Indira Gandhi Centre for Atomic Research, Kalpakkam 603102, India

## Experimental

The chemical composition of modified 9Cr-1Mo steel in the form of 30 mm rolled plate base metal and the weld metal are tabulated in Table 1 (Shankar et al. 2014). Initial heat treatment of the base metal includes normalization at 1323 K for an hour followed by air cooling and subsequently tempering at 1033 K for 45 min followed by air cooling to obtain optimum strength and toughness. Shielded metal arc welding (SMAW) technique (using 20 V and 100 A) was utilized to weld the P91 plates. As the thickness of plates were large, multi-pass welding technique was used to fill the double V groove and joining of the edge prepared base metal plates. Temperature of 423 K was maintained throughout the entire process of welding to avoid hydrogen ingress. The as-welded joints were examined under radiography to ascertain their soundness.

Low cycle fatigue (LCF) specimens were extracted from the welded plates by cutting bars of length 110 mm and 25 mm × 25 mm cross section as shown in Fig. 1a. These bars were further given post-weld heat treatment (PWHT) (1033 K for 3 h and subsequently air cooled) and samples were fabricated (Fig. 1b).

Low cycle fatigue and creep fatigue interaction test were performed in servo hydraulic Instron machine in air environment under total strain-controlled mode. Standard fatigue test procedure and specimens as per ASTM E606 (ASTM-E606, 2012) were followed). Fatigue failed samples subjected to four different waveforms were selected for detailed failure analysis and compared with the as-received condition. These included CC- continuous cycling, 5 min tension compression hold (5TCH), 30 min compression hold (30CH), and 30 min tension hold (30TH). Continuous cycling was performed using a triangular waveform whereas trapezoidal waveform for creep–fatigue interaction

**Table 1** Chemical composition of P91 base metal and weld metal in wt%

| Element | C | Cr | Mo | Ni | V | Nb | N | S | P | Cu | Co |
|---|---|---|---|---|---|---|---|---|---|---|---|
| Base metal | 0.11 | 9.3 | 0.99 | 0.14 | 0.25 | 0.1 | 0.068 | 0.008 | 0.020 | | |
| Weld metal | 0.1 | 9 | 1.0 | 0.7 | 0.17 | 0.06 | 0.055 | 0.012 | 0.009 | < 0.05 | 0.016 |

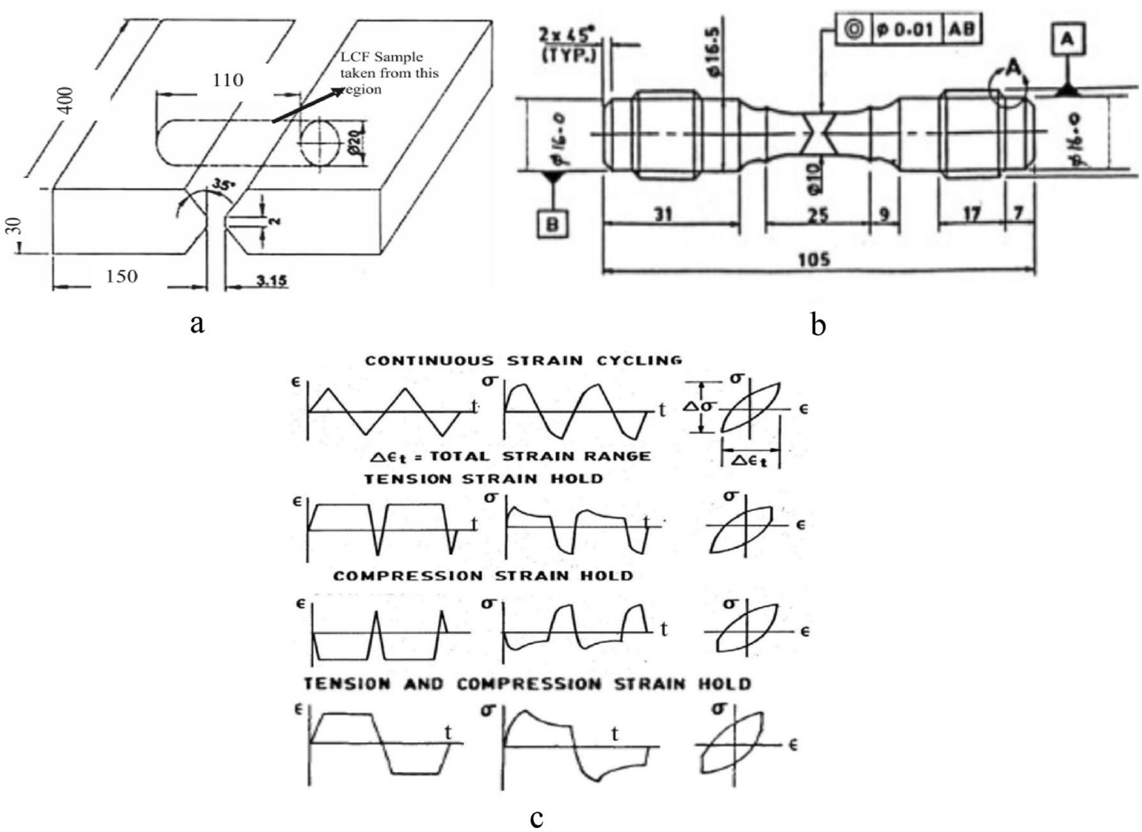


**Fig. 1** **a** Location of LCF specimen extracted from the welded plates, **b** fatigue specimen containing double V weld profile, **c** typical waveforms employed (Shankar et al. 2011)

experiments (Fig. 1c). Total strain amplitude of ± 0.6%, strain rate $3 \times 10^{-3}$ $s^{-1}$ and temperature of 873 K was kept constants for all the four test conditions selected for the present work. Temperature of the sample was maintained well within ± 2 °C to the set temperature.

The cyclically softening nature of P91 steel is represented in Fig. 2a (Vani Shankar 2007, thesis). Among all the waveforms (keeping strain amplitude constant), the pure fatigue (CC) test endured the highest number of fatigue cycles as compared to the conditions that involved the dwell/hold period in either direction or both the directions of the applied strain cycles. This vividly described the involvement of additional creep component in the form of dwell period in every fatigue cycle in causing early fatigue failure. Photographs of failed samples tested under various strain amplitude, temperature and creep–fatigue interaction condition combinations showed shift in failure location as displayed in Fig. 2b.

The longitudinal sections of the fatigue failed samples were polished up to mirror finish using the standard metallographic technique and then etched using Villella's reagent to reveal the microstructure under optical microscope. Microhardness was performed along the same longitudinal section of the fatigue failed samples utilizing Vickers hardness tester. The depth of the indentation by the diamond indenter (using constant load of 200 gf and dwell time of 15 s) was a measure of the extent of local yielding of the microstructural zones. The fatigue failed samples were also prepared for EBSD study by polishing them using colloidal silica of 50 nm particle size. Based on the indent location, EBSD scans were performed at few select regions across the weld joint using step size of 0.2 µm. Schematic of cylindrical specimen containing double V weld joint in different rotation angles about the longitudinal axis were generated as shown in Fig. 2c. This exercise was done for better visualization of the double V weld profile and the main crack/final failure location with respect to the weld profile.

## Results and Discussion

### Initial Characterization

The optical micrograph (Fig. 3) taken on normalized and tempered P91 base metal shows prior austenite grains (PAG) with carbides pinning the boundaries. The microhardness taken across the P91 weld joint and the corresponding micrographs are depicted in Fig. 4. The peak hardness is observed in the all-weld region followed by almost symmetrical dip in the hardness values on the either side which are identified as the heat affected zones and the unaffected base metal. The highest hardness of the weld metal is because of the large solid solution strengthening due to the dissolution of all carbides and the fine microstructure due to fast cooling of the weld metal pool. Adjacent to the fusion zone, where the temperature is around 1473 K (1200 °C) grains are quite large. This causes complete dissolution of the precipitates which

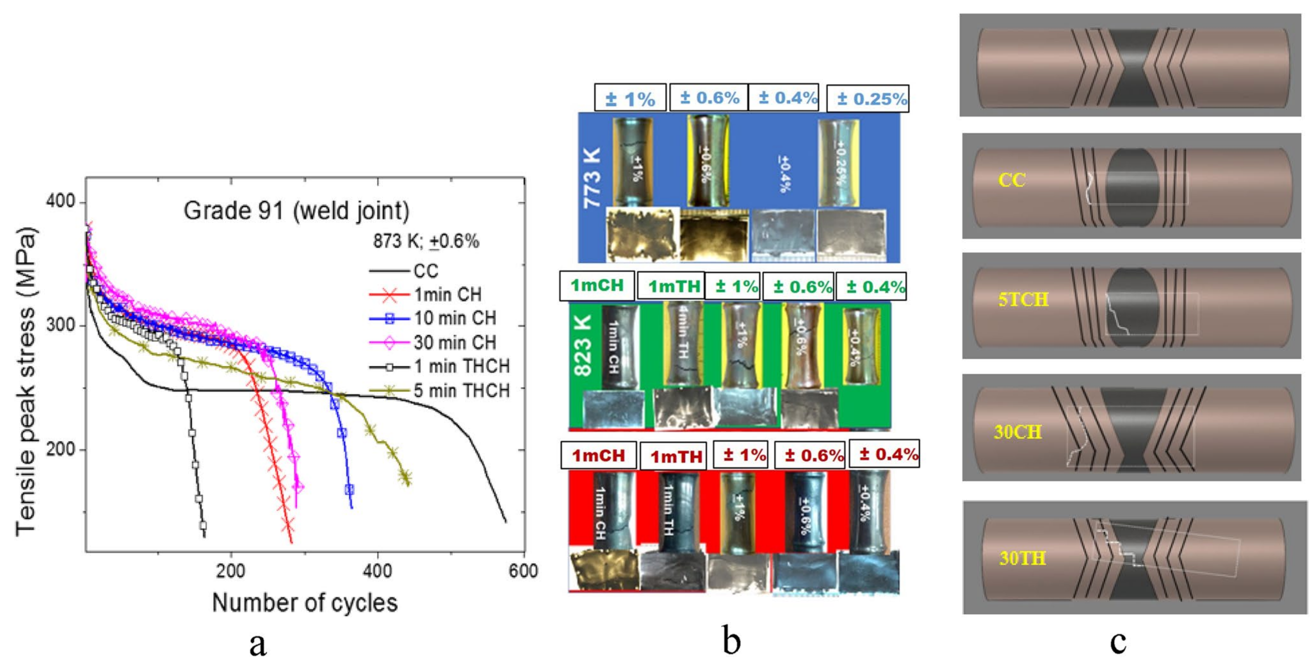


**Fig. 2** **a** Cyclic stress response of P91 WJ tested under CC (without dwell application) and various CFI waveforms, **b** photograph of failed samples tested under various temperature-strain amplitude-waveform-dwell duration combination (Shankar 2007, thesis) and **c** schematic of viewing plane/ longitudinal section depicting different failure locations with change in test conditions

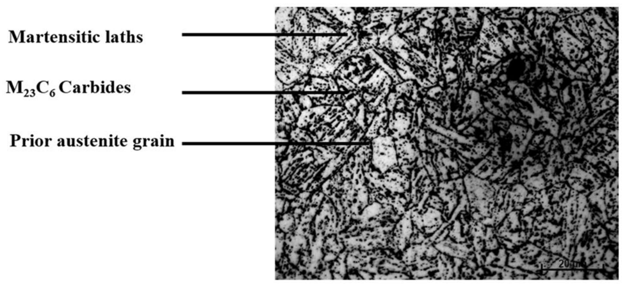


**Fig. 3** Optical micrograph depicting the initial microstructure of P91 base metal in normalized and tempered condition

are responsible for the pinning of the boundaries. As a result, grains grow profusely and form microstructure corresponding to coarse grained heat affected zone (CGHAZ). The high hardness of CGHAZ is mainly due to solid solution strengthening. Adjacent to CGHAZ, fine grained heat affected zone (FGHAZ) forms in the region exposed to temperature just above $AC_3$. Inter-critical heat affected zone (ICHAZ) forms between the temperature range of $AC_1$ which is 865 °C and $AC_3$ which is 1050 °C (Mariappan et al. 2020). Partial dissolution, coarsening of carbides (Yiyu Wang et al. 2018; Chandan pandey et al. 2019) and presence of overtempered α-ferrite leads to the lowest hardness values of ICHAZ as compared to other zones. The unaffected base metal has higher hardness as compared to ICHAZ. The prior austenite grain sizes of base metal, CGHAZ, FGHAZ, ICHAZ using Image-J software were determined as $14 \pm 3$ µm, $34 \pm 12$ µm, $8 \pm 3.5$ µm, $12 \pm 5$ µm respectively in the as- received P91WJ analyzed.

## Microhardness

5 min TCH involves symmetrical loading with a dwell period of 5 min in both compression and tensile direction and the final failure is in the weld metal region. 30 min CH is defined as the dwell period in compression direction alone and the final failure location is in the ICHAZ/FGHAZ interface. It is clearly seen that the microhardness is sensitive enough to pick the microstructural variation information across the P91 weld joint in the as-received condition (Fig. 4a). Hence the same technique was utilized to study the fatigue tested samples exposed to various waveforms and the results are depicted in Fig. 4b. Approximately 200 data points were generated for each test condition at an inter distance of 0.2 mm along the longitudinal section of the well-polished sample. The shaded bands in grey color depict the standard deviation from the average values obtained at same location. The reason for closely spaced microhardness determination was a large heterogeneity of the microstructures within the narrow band of HAZs and to obtain dependable statistical data across the widely varying weld joint of P91. Based on the detailed microhardness and metallographic examination, the various HAZ microstructural zones were categorized as shown by the dotted lines of Fig. 4b. It is clearly seen that hardness of the as-received P91 WJ greatly changed after subjecting to various cyclic waveforms. The level of change in hardness values was different in different microstructural zones of the weld joint. Thus, the weld metal region seemed to drastically soften with the 5 min TCH waveform application when compared to the hardness profile of as-received. The width of the weld metal was off course much wider than as-received because of the different plane of viewing of the same double V weld profile (the reason of which is described in the experimental section). The 30minCH exposed specimen seemed to get further hardened in the HAZ regions and the failure occurred in the ICHAZ/FGHAZ interface.

Several factors may be simultaneously affecting the overall damage and final failure location. Some of them are oxidation assisted cracking and response of surface oxides to further cyclic loadings, mean stress effects, sub structural and carbide coarsening, load sharing-damage accumulation-shift in load transfer mechanism during the course of fatigue life etc. During the analysis it was found that inspite of larger number of surface cracks observed in 30 min CH compared to symmetrical loading 5 min TCH, the overall hardening was observed in 30 min CH and an overall softening under 5 min TCH (as compared to as-received). This clearly reveals that hardening or softening behaviour is caused by the microstructural changes which are independent of the surface oxidation and their cracking behaviour. The microstructural heterogeneity across the P91 weld joint, the multipass welding involved and the interrelated yet independent response of various microstructural zones to various cyclic waveforms reveals that a single hardness line profile may not be sufficient to explain the complex behaviour. A more detailed hardness analysis may therefore be required.

Several factors constitute to the reason for final failure such as exposure temperature that affect dislocation density, precipitate and substructure stability, solid solution strengthening (Panait et al. 2010), sequence of creep and fatigue loading (Aritra et al. 2014), surface oxidation and its response to external loading (Aoto et al. 1994), stress relaxation (Kim and Weertman 1988, Shankar et. al 2014), mean stress effects (Lord and Coffin 1973), nucleation of precipitates (Benjamin et al. 2009) etc. Most of the factors may be inter-related also such as carbide coarsening and substructure stability.

As mentioned in the manuscript, there are several microstructural factors that are simultaneously acting to govern the overall damage and final failure location in P91 weld joint. They are (1) surface oxides, (2) mean stress, (3) sub structural coarsening/refinement, (4) carbide coarsening/refinement. In the scope of the present work it is found

**Fig. 4** **a** Single line profile of hardness taken across as-received (welded + 3hPWHT) weld joint along with corresponding optical micrographs of each zone, **b** microhardness line profiles taken across the weld joint of as-received and two tested conditions (5 minTCH and 30CH)

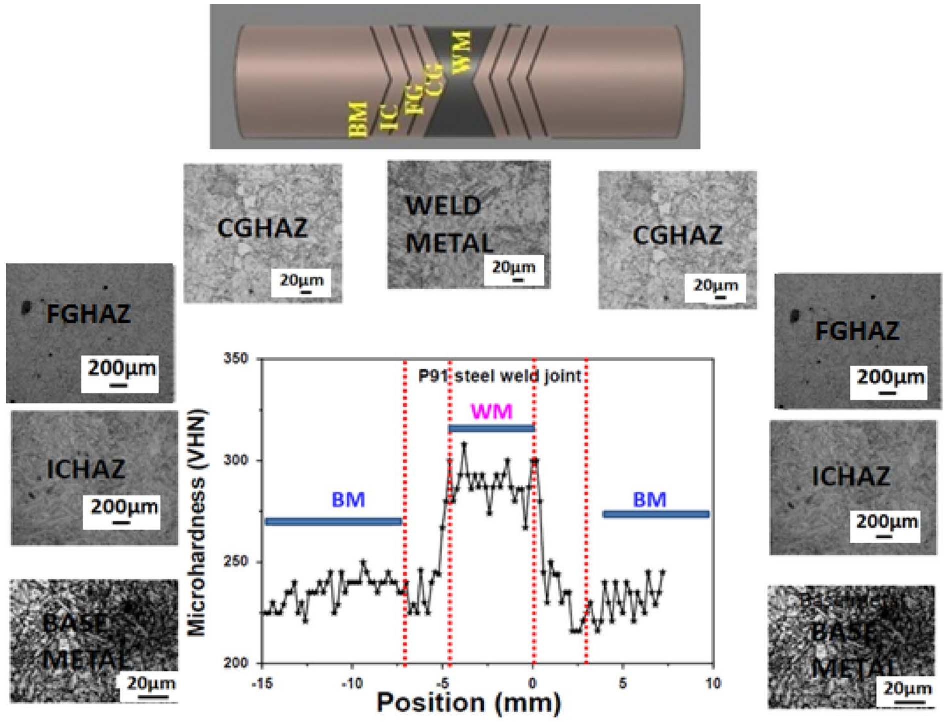


a

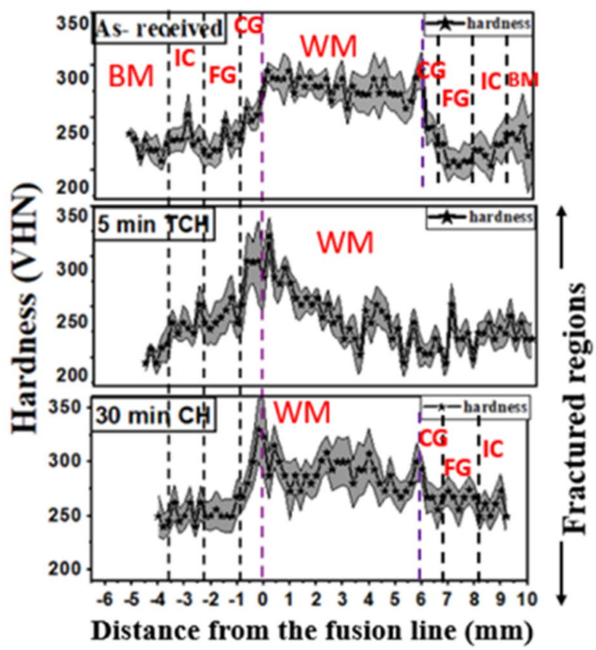


b

that some of the microstructural zones are preferably getting hardened whereas others are preferably softened under different loading waveforms. It is seen that mean stresses developed in the initial few cycles (under unsymmetric loading) diminishes in the subsequent cycles and hence does not affect the final failure. As carbides are responsible for pinning of various boundaries, the stability of substructures are dependent upon the stability of the carbides and hence are interrelated. Thus coarsening/refinement of substructures and carbides (that occurs to different extents in different zones) affects the local mechanical properties (microhardness as in present case). The state of stress at every location of the WJ is continuously changing up to different extents due to the cyclic softening nature of P91. As P91 steel is prone to oxidation, the response of the surface oxides to the loading waveforms is also different (Shankar et al. 2014). To conclude, the final failure is determined by the response of surface oxides, but the microstructural changes is paving the way to the damage enhancement.

The next section discusses the role of one of the few microstructural parameters determined by EBSD technique in affecting the resultant microhardness of the weld joint subjected to different cyclic waveforms.

## EBSD Analysis

It is now well established that grain size plays significant role in determining of the mechanical properties in structural materials (Morris 2001). P91 steel which consists of prior austenite grains partitioned by several types of grain boundaries, the mechanical properties of which is defined more by the finer partitions rather than the prior austenite grain size. Hence EBSD scans were made on some of the representative locations of all microstructural zones of the weld joint, both before and after various fatigue and creep–fatigue interaction tests. Care was taken to truly have one to one correspondence of the microhardness indentation and the EBSD scan with respect to the line profile. Results from only two experiments are represented in Fig. 5. The first classification using EBSD technique is the grain boundary distribution. The boundaries are classified based on their misorientation with respect to the neighboring points. Thus, sub grain boundaries (SGB), low angle grain boundaries (LAGB) and high angle grain boundaries (HAGB)are defined with misorientation to be less than 2°, 2° to 10° and greater than 10° respectively. From the grain boundary maps (Fig. 5a) it is clear that the fraction of LAGBs increases from base metal towards the weld metal. Kernel Average Misorientation (KAM) is an indicator of the strain arising from the presence of geometrically necessary dislocations (GNDs). KAM maps are generated by calculating the average misorientation of less than 5° between center points of the kernel and the neighboring points (Badji et al. 2013). In the present case, 3.5° was considered for the dislocation density analysis. The KAM maps (Fig. 5b) also show drastic increase in the strain intensity from base metal towards the weld metal under both the test conditions.

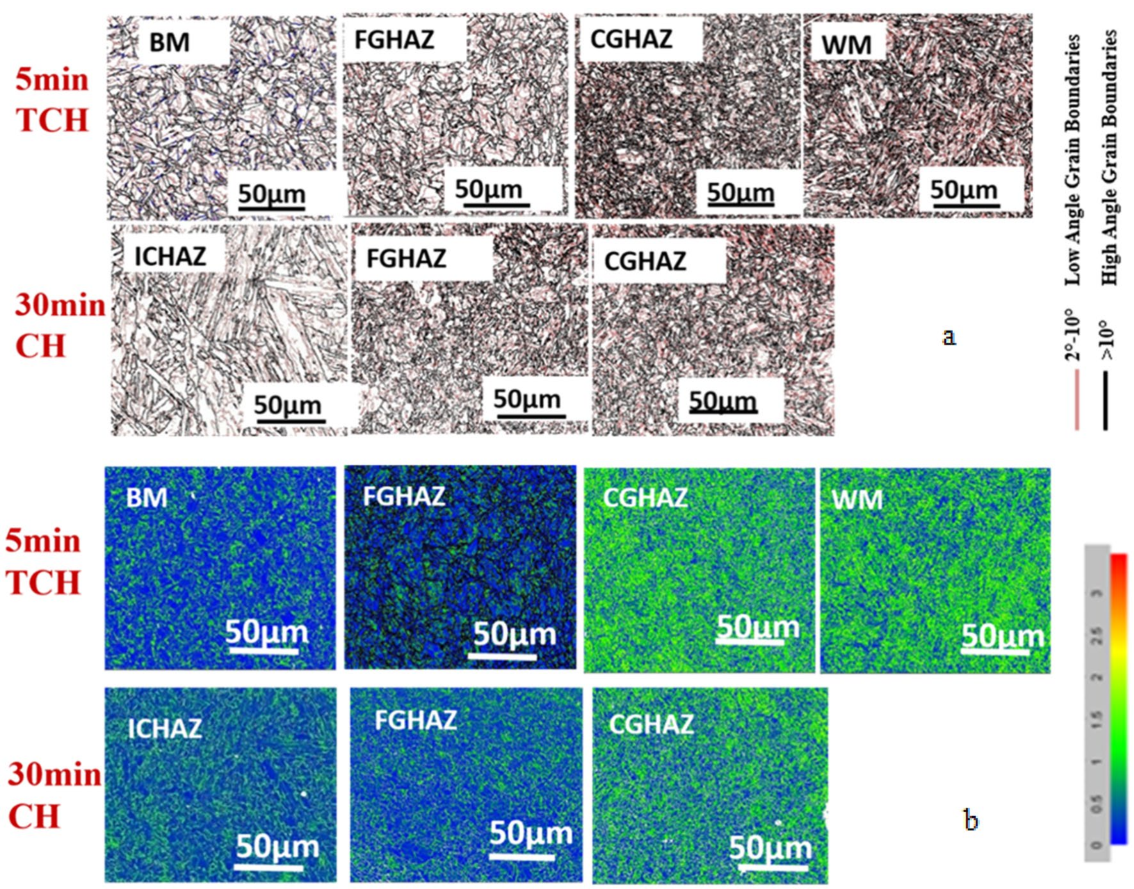


**Fig. 5** Grain boundary maps (**a**) and corresponding KAM maps (**b**) taken across the weld joint after 5 min TCH and 30 min CH tests

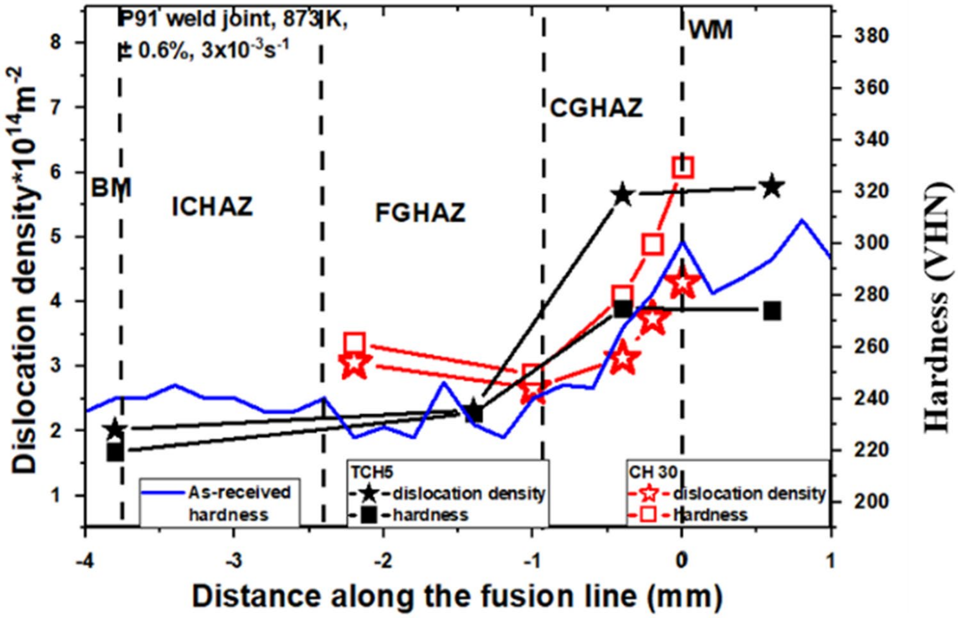


**Fig. 6** Plot of dislocation density versus hardness along the longitudinal section of the weld joint

### Dislocation Density Determination and Correlation with Microhardness

Dislocation density is calculated from the KAM maps using standard available equation which is $\rho_{b=}\frac{\theta i f i}{2b} r_{\ av}$ where $\rho_b$ is boundary dislocation density, $f_i$ is the fraction of subgrain boundaries, $\theta_i$ is the misorientation angle of the subgrain boundary by keeping a threshold of 3.5°, $b$ is the Burgers vector (in present case, Burgers vector for pure iron is considered) and $r_{av}$ is ratio of subgrain size and subgrain volume (Yadav et al. 2016) and the results are plotted against microhardness with respect to the position along the weld joint (Fig. 6). Both microhardness and dislocation density follow the same trend i.e., an increase from the base metal towards the weld metal side. This is true for both the two tests and the as-received conditions. The order of dislocation density observed in the base metal determined by this method matches well with those reported in literature (Panait et al. 2010). The figure clearly confirms that larger is the dislocation density higher is the hardness. The figure also confirms through both microhardness and dislocation density measurement (in few common regions such as FGHAZ, CGHAZ and WM as shown in Fig. 6) that dislocation density is much higher in the FGHAZ under 30minCH as compared to 5 min TCH whereas the dislocation density is much higher in CGHAZ for 5 min TCH as compared to 30 min CH. It must be reiterated that the final failure occurred in the weld metal and the ICHAZ/FGHAZ interface for 5 min TCH and 30 min CH respectively. Thus, it is quite plausible that preferential hardening of the WM over the overall softening of neighboring regions would have caused the WM failure under 5 min TCH. On the other hand, both hardness and dislocation density seem to dip at the interface of FGHAZ and CGHAZ that clearly indicate the shift or redistribution of soft zone from ICHAZ to the interface of CGHAZ-FGHAZ and the final failure would have occurred in the region close to ICHAZ/FGHAZ. However, the picture is still not complete as complete mapping of regions using both EBSD and microhardness is required.

## Conclusions

Cyclic softening/hardening of the constituting microstructural zones of P91 steel weld joint occurred up to different extents under different cyclic waveforms. Overall softening is observed in 5 min TCH whereas overall hardening is observed in 30 min CH which is revealed through the hardness line profiles. Dislocation density measurements through EBSD technique indicated an overall increase in the CGHAZ and WM under 5 min TCH which might be the cause of final failure in the WM region. On the other hand, a dip in the dislocation density and microhardness was observed at the CGHAZ-FGHAZ interface that clearly indicated preferential softening in the region which might be the cause for final failure near the FGHAZ region in the 30 min CH sample.

**Acknowledgements** The authors are thankful to Indira Gandhi Centre for Atomic Research, Kalpakkam and Homi Bhabha National Institute, Mumbai for providing the opportunity to carry out this research.

## References


Aoto K, Komine R, Ueno F, Kawasaki H, Wada Y (1994) Creepfatigue evaluation of normalized and tempered modified 9Cr-1Mo. Nucl Engn Design 153:97–110

ASTM Standard E606/E606M (2012) Standard test method for strain-controlled fatigue testing. Doi: https://doi.org/10.1520/C0033-03

Badji R, Chauveau T, Bacroix B (2013) Texture, misorientation and mechanical anisotropy in a deformed dual phase stainless steel weld joint. Mater Unfoiled 575:94–103

Benjamin F, Maxime S, Alexandra R, Françoise B, André P (2009) Microstructural evolutions and cyclic softening of 9%Cr martensitic steels. J Nucl Mater 386–388:71–74. https://doi.org/10.1016/j.jnucmat.2008.12.06

Farragher TP, Scully S, O'Dowd NP, Hyde CJ, Leen SB (2014) High temperature, low cycle fatigue characterization of P91 weld and heat affected zone material. J Press Vessel Technol 136:2. https://doi.org/10.1115/1.4025943

Hollner S, Fournier B, Lependu J, Caes C, Tournie I, Pineau A (2010) Relationship between microstructure and mechanical behaviour ofthermomechanically optimised 9–12% Cr steels. In: Fracture of materials and structures from micro to macro scale, ⟨hal-00541091⟩

Kim S, Weertman JR (1988) Investigation of microstructural changes in ferritic steel caused by high temperature fatigue. Metall Trans A 19A:999–1007

Klueh RL (2005) Elevated temperature ferritic and martensitic steels and their application to future nuclear reactors. Int Mater Rev 50(5):287–310

Lord DC, Coffin LF (1973) Low cycle fatigue hold time behavior of cast rené 80. Metall Trans 4:1647–1654. https://doi.org/10.1007/BF02666191

Mariappan K, Shankar V, Bhaduri AK (2020) Comparative evaluation of tensile properties of simulated heat affected zones of P91 steel weld joint. Mater High Temp 37(3):1–15

Morris J (2001) The influence of grain size on the mechanical properties of steel. Lawrence Berkeley National Laboratory. Accessed from https://escholarship.org/uc/item/88g8n6f8

Panait CG, Zielinska-Lipiec A, Koziel T, Czyrska-Filemonowicz A, Gourgues-Lorenzon A-F, Bendick W (2010) Evolution of dislocation density, size of subgrain and MX-type precipitates in a P91 steel during creep and during thermal ageing at 600°C for more than100,000. Mater Sci Eng 575A:94–103. https://doi.org/10.1016/j.msea.2013.03.018

Pandey C, Mahapatra MM, Kumar P, Kumar S, Sirohi S (2019) Effect of post weld heat treatments on microstructure evolution and type IV cracking behavior of the P91 steel welds joint. J Mater Process Technol 266:140–154. https://doi.org/10.1016/j.jmatprotec.2018.10.024

Sarkar A, Vijayanand VD, Parameswaran P, Vani Shankar R, Sandhya K, Laha MD, Mathew TJ, Rajendra Kumar E (2014) Influence of prior fatigue cycling on creep behaviour of reduced activation ferritic-martensitic steel. Metall Mater Trans A 45(7):3023–3035. https://doi.org/10.1007/s11661-014-2237-x

Shankar V (2007) PhD thesis titled: Low cycle fatigue and creep-fatigue interaction behavior of modified 9cr-1mo ferritic steel and its weldment, IIT Madras

Shankar V, Sandhya R, Mathew MD (2011) Creep–fatigue-oxidation interaction in Grade 91 steel weld joints for high temperature applications. Mater Sci Eng A 528:8428–8437

Shankar V, Mariappan K, Sandhya R, Mathew MD, Jayakumar T (2014) Effect of application of short and long holds on fatigue life of modified 9Cr-1Mo steel weld joint. Metall Mater Trans A 45A:1390–1400. https://doi.org/10.1007/s11661-013-2108-x

Thomas Paul V, Saroja S, Hariharan P, Vijayalakshmi M (2007) Identification of microstructural zones and thermal cycles in a weldment of modified 9Cr1Mo steel. J Mater Sci 42(14):5700–5713. https://doi.org/10.1007/s10853-006-0704-5

Thomas Paul V, Saibaba S, Vijayalakshmi M (2008) Microstructural stability of modified 9Cr–1Mo steel during long term exposures at elevated temperatures. J Nucl Mater 378:273–281

Wang Y, Li L (2016) Microstructure evolution of fine-grained heat-affected zone in type IV failure of P91 welds. Weld J 95(1):27–36

Wang Y, Kannan R, Li L (2018) Correlation between intercritical heat-affected zone and type IV creep damage zone in Grade 91 steel. Metall Mater Trans A 49A:1264–1275

Yadav SD, Kalácska S, Dománková M, Yubero DC, Resel R, Groma I, Beal C, Sonderegger B, Sommitsch C, Poletti C (2016) Evolution of the substructure of a novel 12% Cr steel under creep conditions. Mater Charact 115:23–31